2. *JANAF Thermochemical Tables*, 2nd ed., Nat. Stand. Ref. Data Service, NBS., Washington, DC (1971).
3. J. Thonstad, *This Journal*, **111**, 959 (1964).
4. H. Ginsberg and H. C. Wrigge, *Metallofizika*, **26**, 997 (1972).
5. A. Silny and T. A. Utigard, in *Light Metals*, pp. 205-211, TMS, Warrendale, PA (1995).
6. P. Drossbach, *Z. Elektrochemie*, **34**, 205 (1928); *ibid*, **42**, 65 (1936).
7. K. Grjotheim, C. Krohn, M. Malinovsky, K. Matiasovsky, and J. Thonstad, *Aluminium Electrolysis, Fundamentals of the Hall-Heroult Process*, 2nd ed., Aluminium Verlag, Dusseldorf (1982).
8. S. Jarek and J. Thonstad, *This Journal*, **134**, 856 (1987).
9. P. Drossbach, T. Hashino, P. Krahl, and W. Pfeifer, *Chem. Ing. Techn.*, **33**, 84 (1961).
10. P. Drossbach and T. Hashino, *J. Electrochem. Soc. Jpn.*, **33**, 229 (1965).
11. K. Vetter, *Electrochemical Kinetics*, Academic Press, Inc., New York (1967).
12. J. Thonstad, *Electrochim. Acta*, **15**, 1581 (1970).
13. E. W. Dewing, *Can. Met. Quart.*, **13**, 607 (1974).
14. M. M. Vetyukov and F. Akgva, *Sov. Elektrochem.*, **6**, 1806 (1970).
15. G. S. Picard, E. C. Prat, Y. J. Bertrand, and M. J. Leroy, in *Light Metals*, pp. 507-517, TMS, Warrendale, PA (1987).
16. E. C. Prat, Ph.D. Thesis, Université de Paris VI (1987).
17. R. D. Armstrong and M. Henderson, *J. Electroanal. Chem.*, **39**, 81 (1972).
18. L. Bai and B. E. Conway, *Electrochim. Acta*, **38**, 1803 (1993).
19. J. R. Macdonald, *J. Electroanal. Chem.*, **223**, 25 (1987).
20. B. Boucamp, *Equivalent Circuit*, University of Twente, The Netherlands (1988/1989).
21. A. Kisza, *Pol. J. Chem.*, **69**, 819 (1995).
22. J. Thonstad, *J. Appl. Electrochem.*, **2**, 315 (1973).
23. R. J. Bowling, R. T. Packard, and R. L. McCreery, *J. Am. Chem. Soc.*, **111**, 1217 (1989).
24. J. O'M. Bockris and A. K. N. Reddy, *Modern Electrochemistry*, Vol. 2, pp. 1004-1008, Plenum/Rosetta, New York (1977).
25. Z. Galus, *Fundamentals of Electrochemical Analysis*, Polish Scientific Publishers, Warsaw (1976).

On the Repassivation Behavior of High-Purity Titanium and Selected α, β, and β + α Titanium Alloys in Aqueous Chloride Solutions

D. G. Kolman*,[a] and J. R. Scully*

Center for Electrochemical Science and Engineering, Department of Materials Science and Engineering, University of Virginia, Charlottesville, Virginia 22903-2442, USA

ABSTRACT

The repassivation characteristics of a titanium thin film evaporated from a high-purity Ti source as well as selected α (commercially pure Ti, Ti-5Al-2.5Sn), β, and β + α titanium alloys (Ti-15Mo-3Nb-3Al, Ti-15V-3Cr-3Al-3Sn, and Ti-3Al-8V-6Cr-4Zr-4Mo) were examined. Both the rapid thin film fracture and scratch depassivation methods were used in aqueous chloride solutions (0.6 *M* NaCl, 5 *M* HCl, 5 *M* LiCl, 5 *M* HCl + 1 *M* $TiCl_3$). Bare surface open-circuit potentials followed the relationship $E(V_{SCE}) = -1.20$ (pH ≈ 0) − 0.043 pH based on the mixed potential established between the anodic Ti/Ti^{+3}, Ti/TiO_2, and water or H^+ reduction reactions. Oxide formation after depassivation was of low overall current efficiency on all titanium materials; a large percentage of the anodic charge following depassivation contributed to dissolution. Consequently, an empirical expression was used to describe the anodic current density decay during repassivation; $i = i_o(t/t_o)^{-m}$. Potentiostatic current transients on rapidly fractured thin film Ti produced plateau bare-metal i_o values greater than 100 A/cm^2 which were below the theoretical ohmic limit, $m = 1.0$ to 1.4 depending on solution and potential and t_o values from 20 to 30 μs. Two anodic Tafel regions and a single cathodic region best described IR-corrected E − log i relationships for bare Ti in all electrolytes. LiCl and $TiCl_3$ inhibited bare surface dissolution but slightly delayed current density decay. Minimal differences between any of the repassivation parameters utilized were observed for selected α, β, and β + α titanium alloys. The similarity was attributed to dominance of Ti^{+3} production in the total anodic charge during repassivation and predominantly TiO_2 formation in the passivating oxides of all alloys.

Introduction

Environmentally assisted cracking (EAC) of metastable β-titanium alloys has been observed in aqueous chloride environments.[1-3] The mechanism by which cracks initiate and propagate is unknown. Mechanical tests on hydrogen-precharged, air-tested, metastable β-titanium (bcc) alloys have suggested that some hydrogen mechanism is responsible for cracking in chloride environments.[4] Conversely, research on many other alloys susceptible to EAC, such as aluminum alloys, has suggested that a dissolution mechanism is responsible for EAC in chloride environments.[5] Previous research in this laboratory has shown that film rupture is required to explain EAC in β-titanium alloys, regardless of the exact mechanism.[6,7] In order to fully evaluate cracking in titanium alloys, whether by a dissolution mechanism, a hydrogen mechanism, or any other EAC mechanism, the bare surface electrode kinetics must be evaluated.

Other researchers have attempted to evaluate the bare surface kinetics on commercially pure titanium[8-14] with limited success, due to a variety of limitations of the potentiostatic test techniques. These limitations have been thoroughly discussed by the authors elsewhere.[15] Bare surface polarization curves on α-titanium (hcp) alloys have been generated by previous researchers[8,14] utilizing Ti-8Al-1Mo-1V (Ti-8-1-1) fractured rods exposed to 12 *M* HCl. However, these tests were ohmically limited, and the fracture speed was relatively slow (approximately 1 ms).[9,14] The effects of alloy composition, cation, solution pH, and $TiCl_3$ were also examined.[14] It was generally found that alloy composition, bulk solution pH, and cation type had little effect on repassivation behavior. It is unclear, however, whether real differences would be revealed if shorter times could be accessed. The true bare surface kinetics on titanium alloys are unknown. Although previous research has examined repassivation behavior of titanium, the data

* Electrochemical Society Active Member.
[a] Los Alamos National Laboratories, Los Alamos, NM 87545.

are limited by relatively slow depassivation rate and ohmic drop in solution.[8-12,14,16] Recently, other researchers have examined the bare surface kinetics on aluminum[17,18] and niobium[19] utilizing thin films deposited on insulating brittle substrates, which are fractured. The fracture and resulting current transient spike occur over approximately 1 to 2 μs, reducing depassivation rate effects.[15] The small amount of bared area reduces the total current and allows a much higher current density to be observed before the ohmic limit is reached. Moreover, the smaller bared area may more accurately simulate the amount of area exposed at a crack tip following film rupture. Therefore, in an effort to better understand the role of crack tip electrode kinetics in EAC of β-titanium alloys, one goal of this research is to examine the bare electrode kinetics on titanium exposed to aqueous chloride solutions through the utilization of fractured titanium thin films. The effects of applied potential on parameters such as bare surface peak current densities, repassivation charge densities, and other repassivation parameters were examined in chloride solutions of differing pH.

EAC has been observed for modern STA (solution heat-treated plus aged) β-titanium alloys exposed to chloride solutions but not for the ST (solution heat-treated) versions of these alloys.[1-3] Also, planar slip has been correlated with the EAC susceptibility of STA alloys.[1-4] The Ti-15Mo-3Nb-3Al alloy examined here exhibited planar slip while Ti-15V-3Cr-3Al-3Sn did not.[4] Thus, it is important to examine the repassivation behavior of the STA (β + α) and ST (β) microstructures of β-titanium alloys separately to discern any differences in their electrochemical behaviors following film rupture that may account for the observed difference in EAC susceptibility. Further, it is of interest to compare the behaviors of the distinct α and β phases in the STA variants of the β alloys to gain insight into the individual components that form the susceptible STA material.

Limited repassivation data exist for β-titanium alloys. Unfortunately, the fractured thin film method cannot readily be used with engineering alloys, due to the difficulty in producing thin films with the identical composition and structure as a bulk multiphase alloy. Thus, a different method must be used to compare the repassivation properties of β-titanium alloys. The manual scratch repassivation test was chosen to compare the repassivation behavior of the alloys of interest. The limitations of this method have been previously discussed by the authors.[15] Although the scratch method is imperfect due to the relatively slow depassivation speed (1 ms) and relatively large scratch area, it may be used qualitatively to discern differences between alloys. If differences between alloys are not observed during scratch testing, it can only be stated that there are no differences between the alloys within the limitations of the test method. The scratch repassivation behaviors of six different alloys were examined: STA and ST Ti-15V-3Cr-3Al-3Sn, STA and ST Ti-15Mo-3Nb-3Al, grade 6 Ti (which simulates α precipitates in the β matrices),[7] and grade 2 Ti (commercially pure).

Experimental

Experimental procedure for manual scratch testing was optimized to minimize shortcomings.[20] Manual scratch testing comprised a variety of α, β, and β + α titanium alloys imbedded in epoxy and mounted on edge so that 0.09 × 0.6 cm was exposed to solution. The small width of the sample (0.09 cm) helped to reduce depassivation speed effects. Electrical connection was made through the back of the sample, opposite the side exposed to solution. The sample was coated with a thin layer of vacuum grease to prevent capacitive current contributions from oxide adjacent to the scratch.[20] Capacitive current contributions from the surrounding oxide has been shown to alter the current response during potentiostatic testing when potentiostatic control of the surface is not maintained.[20] A diamond-tipped glass marker was utilized to scratch through both the vacuum grease and underlying titanium across the 0.09 cm width. Samples were examined with an optical microscope to ensure that no vacuum grease contaminated the scratched region. A Mitutoyo Surftest 401 surface profilometer was utilized to determine the scratch area. The amount of area bared (54.7 μm wide × 0.09 cm scratch length) was obtained by the averaging of many separate scratch tests.[15] A small scratch length was used to minimize depassivation rate effects.[15,53]

Thin film fracture samples comprised a 500 nm thick titanium layer evaporated from a 99.999% titanium source (at 1.8×10^{-7} Torr) onto a glass substrate. A 200 nm thick layer of insulating SiO_2 was sputtered on top of the titanium to prevent capacitive charging[18,20] of the freshly bared surface by its surrounding oxide. A supplemental layer of GLPT insulating varnish was used to ensure insulation of the Ti layer from solution for all open-circuit potential tests, the open-circuit potential being very sensitive to even the smallest of pinholes in the SiO_2. The samples were 1 cm in width, yielding an exposed net-section area of 5×10^{-5} cm^2 upon fracture. Surface roughness of the film was not measured. The film appeared to maintain cohesion with the substrate after fracture, as observed in scanning electron microscopy (SEM). The samples were scored on the glass side of the sample and mounted in the thin film fracture cell.[15] The samples were fractured by impressing a rotationally mounted acrylic breaker onto the bottom of the sample.[15] This method was found to be more satisfactory than guillotining the sample, resulting in far less cell vibration and solution perturbation. Assuming the thin film breaks in a brittle fashion with the crack propagating perpendicular to the thickness of the film, the 500 nm thick layer should be depassivated in 1.6 ns.

Both scratch testing and thin film experiments incorporated a saturated calomel reference electrode (SCE) and a platinized niobium mesh counterelectrode. The reference electrode was placed approximately 50 mm away from the newly exposed metal to allow calculation of the solution resistance, satisfying the condition of being infinitely far from the exposed area.[21]

Samples were held potentiostatically with an EG&G Princeton Applied Research (EG&G PAR) 273 potentiostat. Surface potential and repassivation current were measured with either a Hewlett Packard 54600A or 54601B digital oscilloscope (thin film experiments, 500 ns/data pt), and/or 7090A measurement plotting system (thin film and scratch tests, 100 μs/data pt). The potential and current signals were sampled through their respective analog outputs on the potentiostat.

Potentiostat and reference electrode response have been addressed earlier.[15] In summary, it was found that the response time of the EG&G PAR 273 potentiostat was approximately 5 μs. The deviation of the true potential from the applied potential due to finite potentiostat rise time was found to be far less than that due to ohmic loss in solution. Additionally, the reference electrode imposed no additional limitation on testing beyond that of the potentiostat. Additional tests beyond those discussed in Ref. 15 have been performed. Potentiostatic fractured thin film experiments were performed with an EG&G PAR 283 potentiostat (rise time ~500 ns). No difference was discernible between the current transients obtained with either the EG&G PAR 273 or 283. Thus, the potentiostat rise time does not appear to limit the peak current density as was hypothesized in Ref. 15. Moreover, additional calculations not included in Ref. 15 indicate that double-layer charging contributions are small as determined by current density (i_{max} = 2 A/cm^2 assuming complete double-layer charging in 10 μs) or charge (<0.1% of charge).

Electrochemical impedance spectroscopy (EIS) measurements were performed with a Solartron 1286 electrochemical interface and 1255 frequency response analyzer to determine solution resistance. Solution pH was measured with a Corning 350 pH analyzer.

Solutions of 0.6 *M* NaCl [κ = 0.0521 $(\Omega\text{-cm})^{-1}$] and 5 *M* LiCl [κ = 0.162 $(\Omega\text{-cm})^{-1}$] incorporated reagent-grade NaCl and LiCl, respectively, added to distilled, deionized,

18 MΩ water. Other 0.6 *M* NaCl solutions [κ = 0.0521 (Ω-cm)$^{-1}$] were adjusted to alkaline pH values with reagent-grade NaOH or to acidic pH values with reagent-grade HCl. 5 *M* HCl solutions [κ = 0.602 (Ω-cm)$^{-1}$, calculated pH −1.64[22]) incorporated reagent-grade HCl added to distilled, deionized, 18 MΩ water. $TiCl_3$ was added to the 5 *M* HCl in powder form in an inert, dry atmosphere. The conductivity of 5 *M* HCl + 1 *M* $TiCl_3$ was found to be approximately equal to that of 5 *M* HCl.

The physical metallurgy of the metastable β-titanium alloys, Ti-15Mo-3Nb-3Al (Ti-14.9Mo-2.64Nb-3.15Al, weight percent (w/o)], and Ti-15V-3Cr-3Al-3Sn (Ti-15.0V-2.99Cr-3.14Al-2.81Sn, w/o), have been discussed elsewhere.[4,6,7] Ti-15Mo-3Nb-3Al was solution heat-treated (ST) for 8 h at 871°C (1600°F) followed by an air cool. Ti-15V-3Cr-3Al-3Sn was solution heat-treated for 30 min at 816°C (1500°F) followed by an air cool. Peak aging for both alloys comprised a subsequent single-step heat-treatment at 538°C (1000°F) for 8 h followed by an air cool. The presence of a β + α microstructure, and the absence of other phases, was confirmed by both x-ray diffraction (XRD) experiments, transmission electron microscopy (TEM)/selected area diffraction, and optical microscopy on the STA β alloys.[4] Limited testing was also performed on STA βeta-C (Ti-3.4Al-8.3V-5.9Cr-4.4Zr-4.1Mo, w/o). βeta-C was solutionized at 815°C for 1 h followed by an air cool. The material was aged at 500°C for 24 h followed by air cooling. Scratch tests on grade 6 Ti were performed to examine the repassivation behavior of precipitates in β-titanium alloys. The composition of grade 6 Ti (Ti-5.2Al-2.3Sn) roughly approximates that of precipitates within STA β-titanium alloys.[7]

Potential-current plots were corrected for ohmic loss in solution except for plots where "applied potential" is noted. Metal cation concentrations were assumed to be 10^{-6} *M* for all reversible potential calculations.

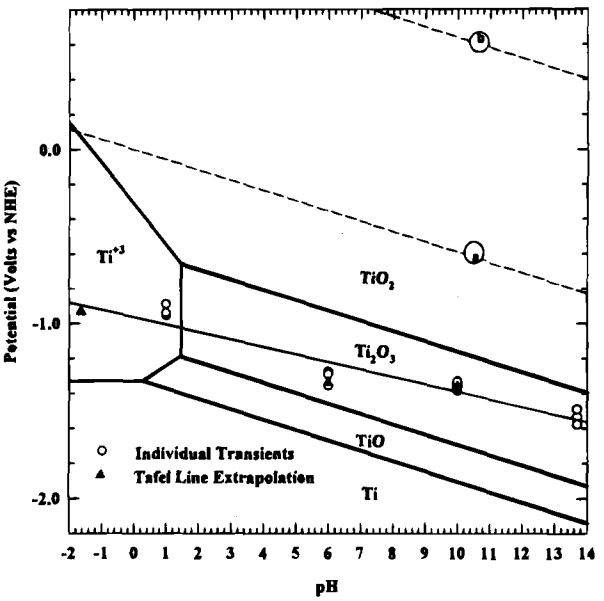

Fig. 1. Bare surface OCP as a function of pH superimposed on the equilibrium potential-pH diagram for titanium considering stability and solubility of anhydrous Ti substances.[24] The open circles are mixed potential minima observed from individual fractured titanium thin film experiments. The filled triangles represent the OCP as determined by extrapolation of anodic and cathodic lines from the bare surface polarization curves. Calculations of equilibrium potential-pH boundary lines assume that all metal cation concentrations equal 10^{-6} *M*. Lines a and b delineate the stable region for water. Limits of the domains of predominance of all dissolved Ti substances are not shown.

Results and Discussion

Bare Surface Open-Circuit Potential Measurements

Figure 1 shows the bare surface open-circuit potentials (OCP) obtained from fractured titanium thin films exposed to 0.6 *M* NaCl solutions of various pH, from pH 1 to pH 13.7. Three individual OCP measurements were obtained in each solution. The bare open-circuit potential was taken as the most negative potential in the OCP transients. Additionally, the intersections of the anodic and cathodic Tafel lines obtained by fitting of the bare surface polarization curves at various pH (discussed later) are also plotted in Fig. 1. In contrast, filmed steady-state OCP range from −0.2 to −0.7 V_{SEC} in deaerated 5 *M* HCl and near-neutral 0.6 *M* NaCl solutions.[6,7] Linear regression of the data in Fig. 1 indicates that the bare surface OCP decreases 43 mV/pH unit [E_{OCP} (V_{SCE}) = −1.20 (pH 0) − 0.043 pH], a slope shallower than that proposed by Beck.[14,23] The linear correlation coefficient for the regression is 0.92, and there is greater than 95% confidence that the magnitude of the slope is less than 50 mV. Good agreement is observed between the individual transients and the values obtained from fitting of the polarization curves.

Beck attempted to determine the dependence of bare surface OCP on pH.[14,23] The depassivation time for these experiments was approximately 1 ms. However, it has been shown that a 1 ms depassivation time alters the apparent bare OCP from the true bare surface OCP.[15] Further, almost all of the tests were performed over a relatively narrow band of pH in concentrated acid, complicating slope determination. Moreover, the activity coefficient of H^+ was assumed to be 1 (*i.e.*, the activity was assumed to be equal to the concentration), which is erroneous in concentrated acid solutions.[22] Thus, the −59 mV/pH result appears to be an overestimate.

The bare surface OCP data shown in Fig. 1 are superimposed on the equilibrium potential-pH diagram using the thermodynamic data compiled by Silverman.[24a] Oxidation of titanium to Ti^{+3} is thermodynamically possible over the observed OCP-pH range. Reduction of water is also thermodynamically possible at these bare metal OCP values. Therefore, Fig. 1 illustrates that the OCP values on bare Ti are mixed potentials established between Ti oxidation and the reduction of water, or hydrogen ions. As such, the slope of −43 mV/pH obtained here is a result of several kinetic and thermodynamic factors changing with pH. If the OCP is a mixed potential that depends on all of the kinetic factors associated with both the anodic and cathodic reactions, as well as their reversible electrode potentials, then a slope of exactly 59 mV/pH unit[23] would not be expected.

Disagreement exists over the details of the electromotive force (EMF)-pH relationships for the Ti-H_2O system.[24-27] Silverman found no evidence for presence of Ti^{+2} ions.[24] Olver and Ross[24b] utilized kinetic and thermodynamic evidence to deduce that the Ti^{+2}/Ti^{+3} equilibrium potential is approximately −2.54 V_{SEC} rather than −0.61V_{SEC} used by Pourbaix.[25,26] Beck argued that the standard equilibrium potential for direct Ti oxidation to Ti^{+3} is −1.451 V_{SEC} and that freshly generated bare Ti may oxidize to TiO_2 at −1.221 V_{SEC} − 0.059 pH.[27] It has also been argued that TiH_2 should form spontaneously upon scratching[27] and that bare titanium is never a thermodynamically favorable surface state at any potential.[26]

Bare Surface Current Density Measurements

Effect of applied potential.—An individual potentiostatic current transient observed during the fracture of a titanium thin film exposed to 0.6 *M* NaCl ($E_{applied}$ = 0 V_{SCE}) is seen in Fig. 2. A peak current of 8.75 mA was recorded. This corresponds to a current density of 175 A/cm^2. Comparable current densities have been observed on fractured aluminum[17,18] and niobium[19] thin films. The anodic bare surface current density is approximately eight orders of magnitude larger than that seen at similar potentials at steady state.[6,7] Also, the measured anodic current density is approximately 100 to 1000 times larger than that observed from tests which utilized different depassivation methods.[8,10-12] In contrast to previous repassivation meth-

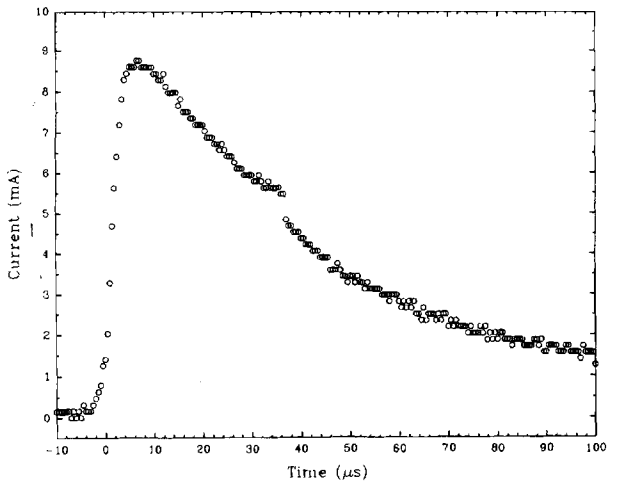

Fig. 2. Measured current repassivation transient for a fractured titanium thin film electrode exposed to 0.6 *M* NaCl at E_{app} = 0 V_{SCE}.

ods, fractured thin films yield peak current densities that are neither limited by voltage drop in solution[a] nor by depassivation speed.[15] (The theoretical ohmic limit for the experiment of Fig. 2 is 23 mA.) Thus, fractured thin film data appear to be a more accurate characterization of the bare surface dissolution plateau for titanium.

Current transients at selected applied potentials are plotted in Fig. 3 on a log i - log t scale. The current transient of Fig. 2 is the 0 V_{SCE} experiment in Fig. 3. Each transient is a combination of two sets of data recorded at different sampling rates from the same test, in order to examine current decay over five time decades. Current decay is plotted from the peak current observed. The time of the peak current (2.5×10^{-7} s) is taken to be half of the sampling frequency. The peak anodic bare surface current densities decrease with decreasing potential due to decreasing overpotential for anodic dissolution. The transients at the most positive potentials in Fig. 3 (0, −0.3, and −0.9 V_{SCE}) remain net anodic over the duration of the test. Experiments at intermediate potentials (−1.1 and −1.525 V_{SCE}) are initially anodic but become cathodic as repassivation occurs. This is due to the fact that the applied potential is anodic to the bare surface OCP (Fig. 1) but cathodic to the OCP of the filmed surface (−0.2 to −0.7 V_{SCE}) at steady state. Tests at the most negative potentials (−1.8 V_{SCE}) remain net cathodic throughout the length of the test, also consistent with Fig. 1. In fact, little change is observed following fracture. The surface has been shown to never remain film-free at equilibrium, even at potentials below −2 V_{SCE}. Under these conditions, TiH_2 may be the equilibrium surface state instead.[26,27]

[a] We strictly define the term "ohmically limited" to describe the instance where the current reaches the ohmic limit. Tests that are not ohmically limited may still be ohmically affected, *i.e.*, may experience ohmic loss in solution.

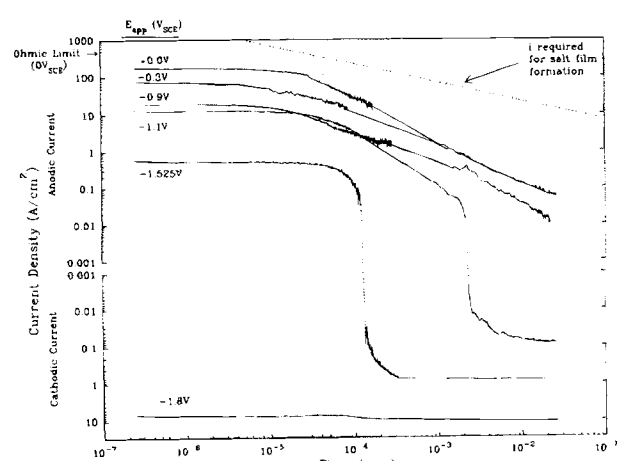

Fig. 3. Individual current transients of fractured titanium thin films at the indicated applied potentials in 0.6 *M* NaCl. Each current transient is a combination of two sets of data acquired from the same experiment at different acquisition rates. The theoretical ohmically limited maximum current density is indicated. The time required at constant current density for salt film formation assuming semi-infinite linear diffusion from a planar electrode is indicated.

Other investigators have attached significance to the length of the current density plateau at the earliest times following depassivation.[10-12] Models have been developed[28] and used[10-12] which attribute the plateau length to the time required for the formation of the initial monolayer of oxide. However, experimental artifacts have been shown to affect the length and magnitude (current) of the plateau in ohmically limited[9,15,16] or depassivation speed limited experiments.[15] In the absence of ohmic or depassivation speed limitations, as in fractured thin film tests, it may be possible that the 10 to 50 μs plateau length may be indicative of the time required for monolayer chemisorbed oxygen or oxide formation. Further study would be required to confirm this hypothesis.

Charge density.—The charge density passed following fracture was calculated by integration of current density-time curves up to 30 ms (Table I). For all of the charge densities in Table I, the net current remained anodic for the entire 30 ms of data acquisition, thereby allowing integration over this time. At potentials below −0.6 V_{SCE}, charge densities are not reported, due to significant contribution from cathodic reactions on the repassivating surfaces at longer time periods which could not be accounted for accurately. For instance, at 0 V_{SCE} in 0.6 *M* NaCl, the charge density was found to be 25 mC/cm² after 30 ms. The calculated charge density, an average of multiple tests, is actually an underestimate of the true anodic charge density, because it neither incorporates unaccounted anodic current equaling the cathodic current supplied by the bare surface nor anodic current data after 30 ms. If it is assumed that the current decays with a slope of −1.09 on the log i − log t plot until the steady-state current passive density[6,7] is reached, the anodic charge density would be almost 50% greater than obtained after 30 ms at all applied potentials reported in Table I. The charge densities required for oxides of steady-state thicknesses formed at −0.6, −0.3, and 0 V_{SEC} in 0.6 *M* NaCl range from 1.2 to 3.2 mC/cm², assuming steady-state thicknesses that increase 2.3 nm/V (as determined by EIS[6,7]), a 0.52 nm monolayer thickness[29] assumed to exist below −0.37 V_{SEC}, and 3.4 g/cm³ oxide density.[29] The oxide thickness on titanium following repassivation has been found to be consistent with these.[29] The resulting overall current efficiencies after 30 ms are less than about 13%. The extrapolated anodic charge densities for complete repassivation, assuming the current decays with a slope of −1.09 on the log i − log t plot at −0.6, −0.3, and 0 V_{SCE} in 0.6 *M* NaCl, range from 27 to 32 mC/cm². The overall current efficiency for oxide formation after decay to steady state would be less than 10% for the applied potentials reported in Table I.

Table I. Comparison of charge densities passed (mC/cm²) following fracture of titanium thin films up to 30 ms. Charge densities are obtained by integration of the current density-time transient and represent an average of at least two experiments. (Charge density to form steady-state oxide = 1.2 to 3.1 mC/cm² for steady-state oxide thicknesses at −0.6 to 0 V_{SCE}.)

Potential	5 *M* HCl	0.6 *M* NaCl	0.6 *M* NaCl, pH 10
0.5 V_{SCE}	36	—	—
0 V_{SCE}	30	25	28
−0.3 V_{SCE}	28	16	—
−0.6 V_{SCE}	—	17	16

Therefore, the large majority of repassivation charge goes toward dissolution of titanium for all of the conditions of Table I (probably as Ti^{3+} or TiO^{+2}, as confirmed elsewhere from scraped disk/ring experiments[27]) and not into oxide formation ($Ti + 2H_2O \rightarrow TiO_2 + 4H^+ + 4e^-$). Therefore, the conclusion that a large portion of the charge passed following Ti film rupture in chloride solutions goes toward dissolution is well supported.[27,30] However, the rapid fracture thin film technique gives a more accurate assessment of overall current efficiencies for oxide formation.

Previous theories have suggested that the entirety of the dissolution occurs during the plateau current density region (Fig. 3) at early time.[10-12] The charge passed during the subsequent current decay was attributed to oxide thickening.[10-12] The depth of metal penetration by dissolution in 20 μs (Fig. 3) could reach 1.6 nm, possibly undercutting islands of oxide attempting to cover the bare surface as reasoned before.[9] However, this effect could only partially account for low efficiencies seen. The charge density passed during each subsequent time decade is roughly equal, because the current decay is nearly logarithmic.[15] Therefore, significant dissolution must take place for the entire duration of the current decay transient because nearly 90% of the total charge goes toward dissolution. It is probable, therefore, that a high concentration of Ti^{3+} or TiO^{+2}, depending upon applied potential, will be present in a crack tip solution following film rupture. Since hydrolysis is probable, the hydrolysis product of Ti^{+3} (*i.e.*, $Ti(OH)^{2+}$) may be present (Appendix A).

Current decay.—The general expression where i is current density (A/cm^2), i_0 (A/cm^2) is the peak bare surface current density, t is elapsed time at $t>t_0$ or $t = t_0$ for $t<t_0$ (s), and t_0 (s) and m (unitless) are constants, was utilized for analysis of the current decay following depassivation[31]

$$i = i_0\left(\frac{t}{t_0}\right)^{-m} \qquad [1]$$

Table II shows the constants obtained by linear regression of the more positive applied potential experiments. A typical fit of log i *vs.* log t is seen in Fig. 4 (0.6 *M* NaCl, E_{app} = 0 V_{SCE}, linear correlation $r^2 \approx 0.998$). Fitting was performed from 10^{-4} to 0.03 s. The transients fitted in Table II were chosen for fitting because they remained net anodic over the entire acquisition time. Thus, they were less influenced by cathodic reactions on the repassivating surface than those at more negative potentials and may be considered to represent the anodic repassivation behavior on titanium in 0.6 *M* NaCl. It is seen from Table II that both t_0 and m are similar for the various potentials. This suggests that the repassivation behavior (oxide reformation and dissolution) at the different potentials is similar at times greater than 10^{-4} s following fracture. Moreover, m, which represents the slope of the transient on the log i - log t plot, is seen to be greater than one. It has been shown that m cannot be greater than one if the high field approximation is applicable.[16] The high field approximation[32] has been used to model the current decay recorded during potentiostatic repassivation tests.[8,10-12,16] However, the high field approximation is inappropriate for modeling the repassivation of titanium exposed to chloride solutions, because the model assumes that current is entirely due to oxide thickening. Instead, the observed anodic current transient is mainly due to dissolution as shown.[15] Thus, the

Table II. Comparison of parameters obtained by fitting of current transients at different potentials (0.6 *M* NaCl) to Eq. 1. Values for *m* are ± 0.04.

Potential	t_0 (s)	m
0 V_{SCE}	2.05×10^{-5}	1.14
0.3 V_{SCE}	1.76×10^{-5}	1.05
−0.6 V_{SCE}	2.56×10^{-5}	1.08

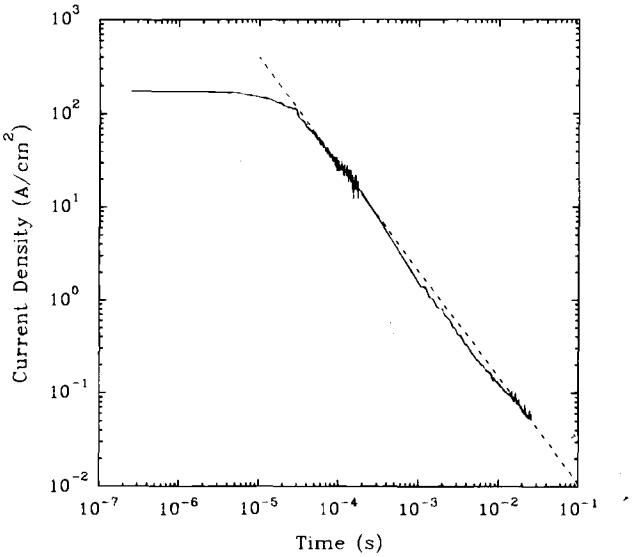

Fig. 4. Typical fit of log $i = -m \times \log t$ from Eq. 1 to a titanium thin film repassivation transient (E_{app} = 0 V_{SCE}, 0.6 *M* NaCl). The *m* parameters from such fits are seen in Table II. The linear correlation coefficient $r^2 = 0.998$.

fact that m is greater than one is not unreasonable. It has been hypothesized that when the current efficiency for oxide formation is low, increasing oxide perfection instead of oxide thickening accounts for the roughly logarithmic current decay.[33] Such a scenario may be valid for the case of titanium exposed to chloride solutions.

The current density required for salt film formation ($i = 2.2\ t^{-1/2}$)[9] is plotted in Fig. 3. The current density transients are generally orders of magnitude below the current-time product required for salt film formation. Thus, the current decay is attributable to oxide perfection and not salt film formation. Beck hypothesized that the steep decay (slope ≈ -2 on log i − log t plot) following the current density plateau observed in potentiostatic repassivation experiments might be attributable to salt film production.[34] However, the repassivation experiments performed by Beck were ohmically limited and Burstein and Davenport have shown that ohmic drop in solution can yield $m > 1$.[16] Beck also formulated an extensive theory in the late 1960s [the mass transport kinetic (MTK) model] which argued that cracking of titanium alloys in chloride environments was due in part to the formation of a salt film near the crack tip.[23,34,35] The salt film formation hypothesis was subsequently weakened by Beck's later calculations and by experiments incorporating anions which form salts with Ti^{+3} of widely varying solubility[9] which yielded similar repassivation behavior. Thus, it appears that salt film formation does not take place upon repassivation of titanium at the potentials and for the electrode geometry examined here.

Polarization behavior.—The current densities at different potentials can be plotted to produce polarization curves at various times following depassivation (Fig. 5). Surface potentials have been corrected for ohmic drop in solution using the calculated solution resistance[21] (discussed later). Individual data points are shown for the peak current density data only. It is seen that current densities on freshly exposed titanium are 4 to 9 orders of magnitude larger than that seen at steady state. Extremely large current densities are seen to occur at short times following film fracture. However, these large current densities are short-lived and rapidly decay toward that seen at steady state. This is seen from the family of polarization curves at times following the peak current density. Moreover, it is seen that the OCP increases with time, toward that seen at steady state, as expected.

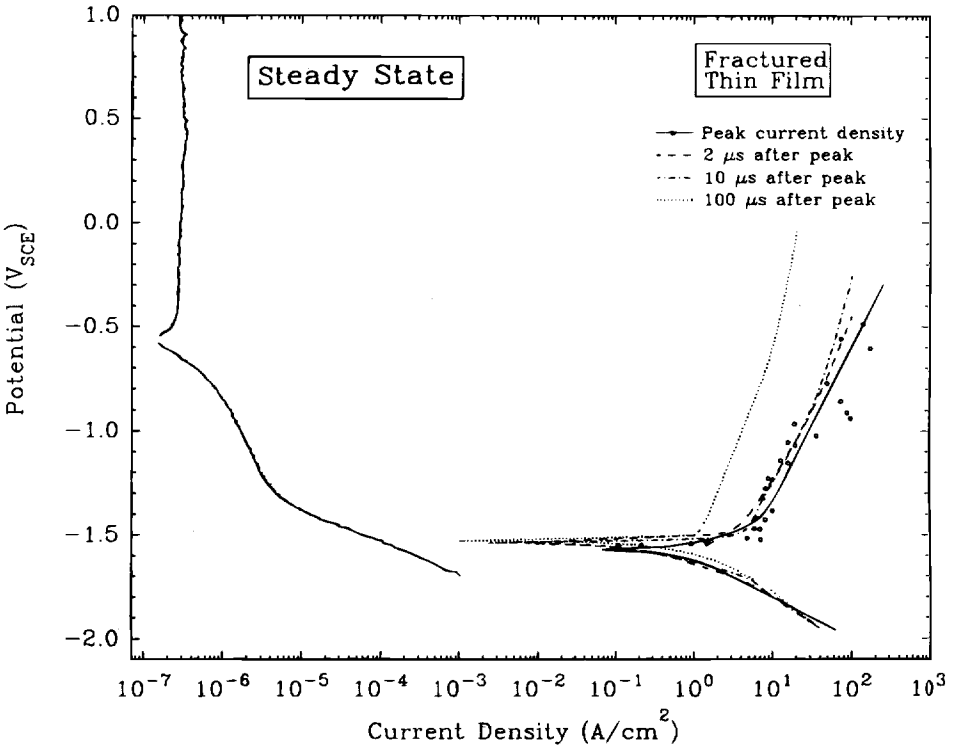

Fig. 5. Comparison of the bare surface (peak current density) polarization curve, polarization curves at various times following depassivation of fractured titanium thin films, and the steady-state polarization curve on grade 2 titanium (0.05 mV/s scan rate) in 0.6 *M* NaCl. Only individual data points for the peak current density curve are shown. Polarization curves are lines qualitatively drawn as the best fit.

The theoretical ohmically limited current density can be calculated from the formula shown. (Assuming that the oxidation charge-transfer resistance $R_{ct} << R_S$ for a bare metal, this calculation gives the theoretical ohmically limited current density.)

$$i = \frac{E_{app} - E_{bare\ OCP}}{(R_s)(\text{Area})} \quad [2]$$

These current densities are compared to the bare surface polarization curves for 0.6 *M* NaCl and 5 *M* HCl in Fig. 6. (The data points in Fig. 6 are the averages of the current densities of multiple tests for a given applied potential.) The solution resistance is calculated from[21]

$$R_s = \left(\frac{1}{2\pi\kappa b}\right) \ln\left(\frac{4b}{a}\right) \quad [3]$$

where R_s is the solution resistance (Ω), κ is the solution conductivity $(\Omega\text{-cm})^{-1}$, a is one-half of the bared area width (cm), and b is one-half of the bared area length (cm). For 0.6 *M* NaCl solutions, R_s is calculated to be 69.0 Ω. This is in excellent agreement with the solution resistance determined by current interrupt measurements (68.0 Ω) and EIS (66.6 Ω). The peak current densities fall below the theoretical ohmic limit.[15] It is reasonable to argue, therefore, that the fractured thin film tests are not ohmically limited. A plot of measured current *vs.* applied potential[15] displays a nonlinear slope, thus confirming this conclusion.

Two Tafel region anodic behaviors.—For the anodic portion of the ohmically corrected bare surface polarization curve (Fig. 7), two different regions are observed, a region of relatively low slope near the bare OCP and a region of relatively high slope at more noble potentials. The current densities obtained during testing are the net current densities supplied by the potentiostat. Far above the OCP, these current densities are a good approximation of the anodic current density, because the cathodic current density supplied by the bare surface, which cannot be measured, is insignificant compared to that supplied by the potentiostat. However, near the OCP, the contribution of the cathodic current is significant compared to the anodic current. The net current measured is substantially less than the true anodic current and yields a region near the OCP wherein the slope is shallow compared to the slope far away from the OCP. On initial inspection, it appeared that this situation might explain the distinct regions of the anodic polarization behavior. A nonlinear least squares fit of the data using one anodic Tafel slope and one cathodic Tafel slope, however, suggests that this is not the case (Fig. 7a and b).[b] Two distinct anodic regions are observed and a fit with two Tafel slopes describes the data accurately in 5 *M* HCl, 0.6 *M* NaCl, and 0.6 *M* NaCl at pH 10. A single Tafel slope is seen for the cathodic data in all cases. Moreover, because the cathodic data are linear (on the E - log i plot) over the same current densities (5 to

[b] Reversible potentials were fixed during fitting. Exchange current densities and Tafel slopes were allowed to vary.

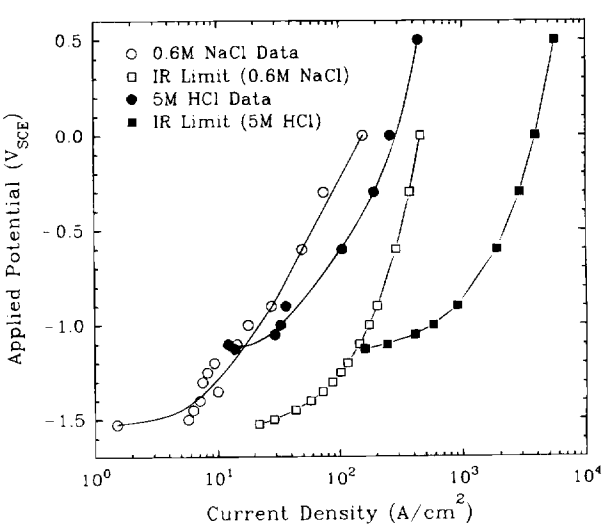

Fig. 6. Comparison of the average current densities at their respective applied potentials to the theoretical ohmically limited current density (Eq. 2) for the solutions shown.

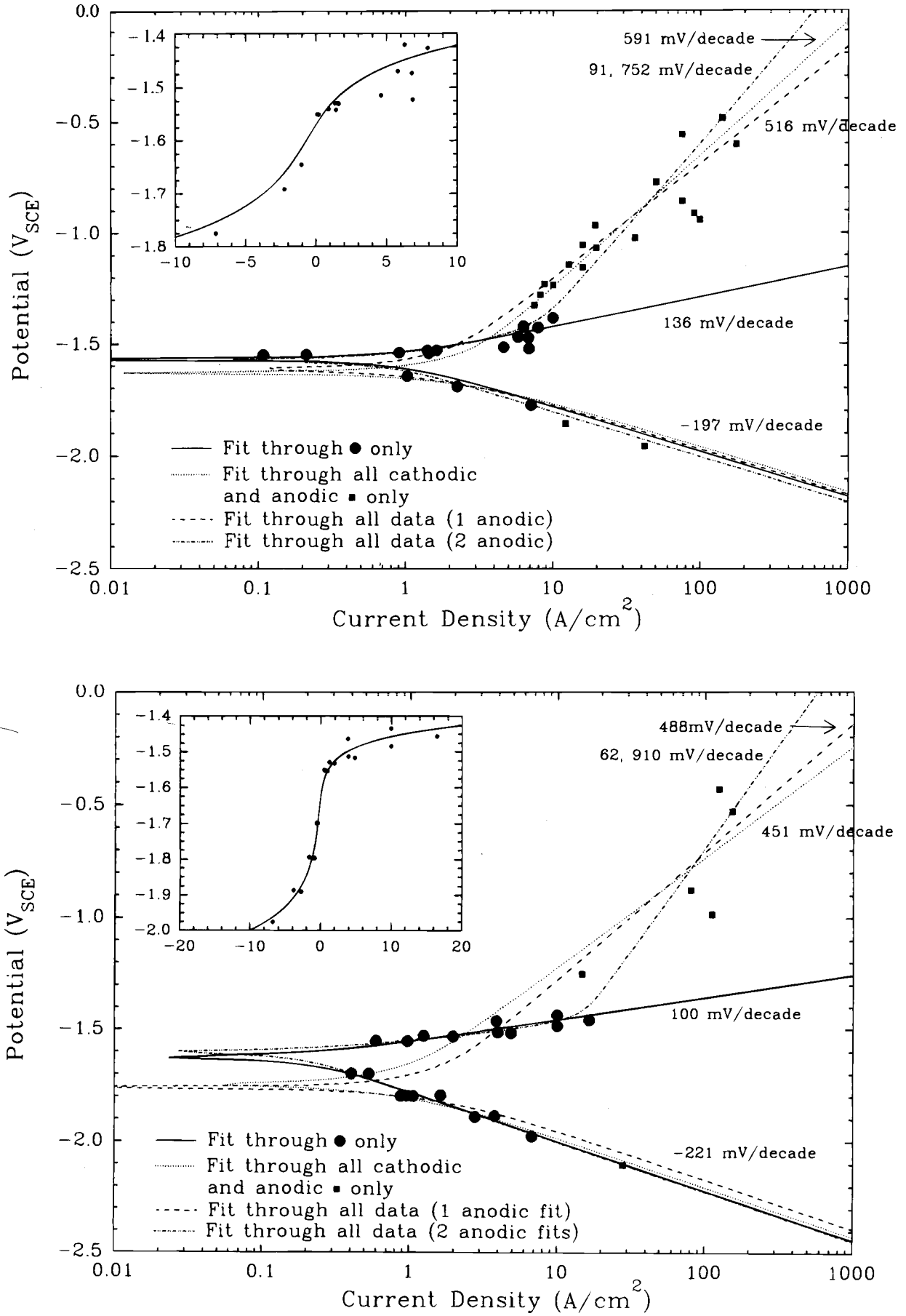

Fig. 7. Fractured titanium thin film bare surface polarization data in (a, top) 0.6 *M* NaCl and (b, bottom) 0.6 *M* NaCl at pH 10. Various nonlinear least squares fits are shown. Reversible electrode potentials were fixed during fits to Tafel slopes and exchange current densities. Inset shows *E-i* relationships in the vacinity of the mixed potential.

100 A/cm^2) where the anodic data display two different slopes, it does not appear that the anodic region of the steep slope is the result of some artifact of testing, such as potentiostat response, slow surface wetting, or ohmic shielding by the freshly broken-off thin film end.

Others have seen the double anodic slope phenomenon with scratched iron and stainless steel electrodes.[36,37] The shallow sloped region was attributed to Tafel behavior.[36,37] The region of steep slope has been explained as a scratch speed-limited regime.[15] Other work with fractured Ti-8-1-1 rods in 12 *M* HCl appears to show two regions as well.[8] The region of steep slope, however, appears to be a region of ohmic limitation. As discussed earlier, the fractured thin films are ohmically corrected and are neither limited by voltage drop in solution or by depassivation speed.[15] Thus, it may be that the region of steep slope is actually indicative of the true kinetic response of the surface. In conventional electrochemistry, dual Tafel slopes are often a result of a change in kinetic rate-determining step or change in reaction intermediate surface coverage. However, the bare metal kinetic response cannot continue to be of low Tafel slope (*i.e.*, a Tafel slope of 100 mV/dec or so) at 0 V_{SCE}, because unreasonable current densities exceeding 10^{10} A/cm^2 would be required. Thus, some limiting factor, which is not a known artifact of the test method, may play a role in limiting the current density. This limiting factor would produce a steep slope in order to maintain attainable current densities in the 0 V_{SCE} potential range. The mass transport-limiting current density for reduction of water is approximately 3000 A/cm^2 at 10 ms. Thus water transport can be eliminated as a possible limiting factor.

High Tafel slopes may be explained at the very high current densities measured here. If the free energy of the initial state becomes high enough (a possibility for bare titanium which is extremely unstable), the reaction becomes essentially activationless.[38,39] Further increases in applied potential would not produce current density increases that are exponential with overpotential. It has been suggested that an activationless reaction may possibly control the apparent Tafel behavior in light of the absence of other known limiting factors.[40] The reader should recognize that many of the common assumptions utilized for steady-state electrochemical kinetics may not apply to metal dissolution at such high rates. Little experimental work is available to validate assumptions of conventional Tafel slopes.

Effect of solution chemistry.[c]—*Variation of pH.*—Individual current transients arising from thin film fracture tests in chloride solutions of different pH (5 *M* HCl, 0.6 *M* NaCl, and 0.6 *M* NaCl adjusted to pH 10) at similar anodic overpotentials are seen in Fig. 8. 5 *M* HCl resulted in a slightly greater bare surface peak current density than that in neutral and pH 10 solutions at similar overpotentials when corrected for ohmic loss in solution. None of the curves shown are at the theoretical ohmic limit (Fig. 6). Repassivation is fast for all anodic transients, with approximately logarithmic current decay, even in 5 *M* HCl. This is not surprising as repassivation of titanium has been observed by others in 12 *M* HCl.[14] Transient morphology is similar in neutral and pH 10 NaCl solutions. However, 5 *M* HCl transients appeared to have a slightly faster repassivation rate (larger *m* values). Table III, which shows repassivation parameters (at identical applied potentials, 0 V_{SCE}) fitted to Eq. 1, confirms these observations. The peak current densities from individual transients may be plotted *vs.* potential to generate bare surface polarization curves (see Fig. 9). Potentials are ohmically corrected. It is seen that for a given overpotential, bare surface anodic and cathodic polarization behaviors are qualitatively similar in solutions of widely differing pH, with the more acidic solutions displaying higher current densities for a given overpotential. The bare surface polarization curve of titanium in all of the solutions has two distinct anodic regions and one cathodic region. Additionally, the polarization curves at various times following depassivation (similar to that seen in Fig. 5) appear comparable as well, with the current densities decreasing over time at similar rates in all solutions.

[c] This paper focuses on chloride solutions. It should be noted that fractured titanium thin film tests in 0.6 *M* and 1 *M* Na_2SO_4 revealed behavior indistinguishable from that in 0.6 *M* NaCl.

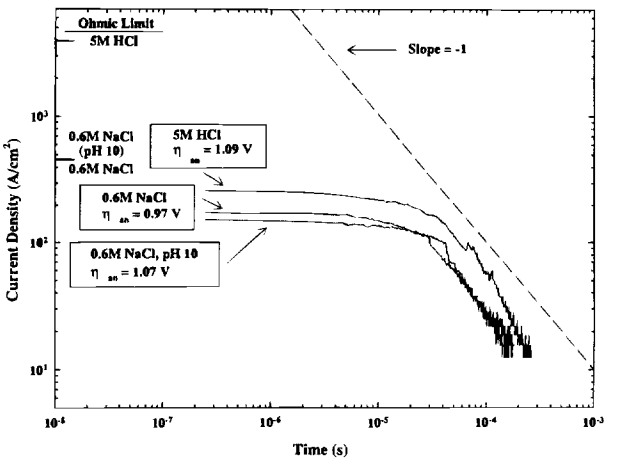

Fig. 8. Individual fractured titanium thin film current transients in different solutions. The current transients have similar anodic overpotentials (with respect to open circuit) at the peak current density when corrected for ohmic loss in solution. The applied potential for all tests was 0 V_{SCE}. Ohmically limited current densities for each test (Eq. 2) are shown on the left side of the plot.

Anodic charge densities passed following depassivation in different pH solutions are compared in Table I. As in the neutral solution, the average anodic charge densities passed in both 5 *M* HCl and 0.6 *M* NaCl adjusted to pH 10 far exceed that required for oxide film formation. Thus, in all these solutions, the large majority of anodic charge goes toward dissolution with only a small fraction utilized for film formation. Because the 0 V_{SCE} experiments have roughly similar anodic overpotentials (Fig. 8), the anodic charge densities may be compared. It is seen that the charge densities in the different solutions are statistically similar, as the charge density data revealed some scatter (± 20%). In summary, anodic charge densities, as a function of overpotential, show little dependence upon solution pH. Similar behaviors in solutions of widely varying pH argue against a dissolution mechanism controlling EAC of β-titanium alloys, as cracking is observed when acidic crack tip chemistries are present, but not when alkaline chemistries exist.[41]

Anodic and cathodic Tafel slopes were obtained by nonlinear least squares fitting of the peak current density data. As with the neutral bare surface polarization curve (Fig. 7), the polarization curves from 5 *M* HCl and pH 10 solutions displayed two distinct anodic regions. The two anodic and one cathodic Tafel slopes, OCPs, and corrosion current densities in the three solutions are compared in Table IV. The calculated OCPs are in good agreement with those obtained from individual thin film fractures (Fig. 1). Additionally, the corrosion current density was found to be greater in the acidic solution than in the neutral or basic solutions. The cathodic water reduction exchange current densities are orders of magnitude larger than that

Table III. Comparison of parameters obtained by fitting of current transients from fractured thin film tests in different solutions (E_{app} = 0 V_{SCE}) to Eq. 1. Values for *m* are ± 0.04.

Solution	t_0 (s)	*m*
5 *M* HCl	2.99×10^{-5}	1.36
0.6 *M* NaCl	2.05×10^{-5}	1.14
0.6 *M* NaCl, pH 10	2.04×10^{-5}	1.16

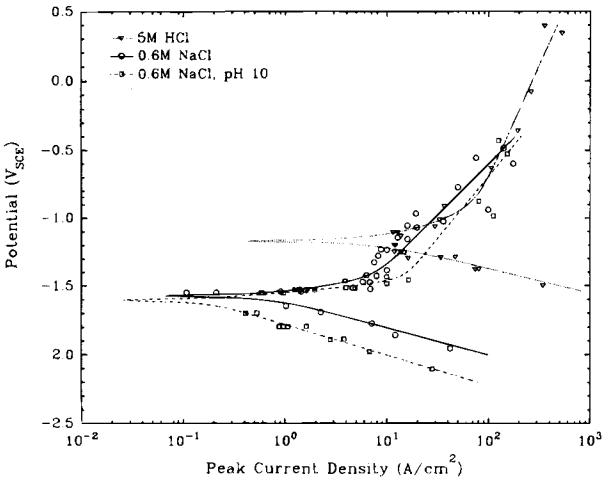

Fig. 9. Bare surface polarization curves (peak current densities) of fractured titanium thin films in various environments.

seen on TiO_2-covered titanium.[7] Exchange current densities are many decades of current removed from the data and are not reported due to resulting uncertainties. Also, high anodic slopes are only approximate in 5 *M* HCl and pH 10 solutions, because fewer data points were obtained in the steep portions of these curves.

The low anodic Tafel slope may be indicative of conventional Tafel behavior. Caprani *et al.* have proposed a general anodic reaction mechanism of $Ti \rightarrow (Ti^{3+})_{ads} \rightarrow Ti^{3+}$ in acidic chloride media for the production of trivalent titanium.[42-46] The observed anodic Tafel slopes vary from 62 mV/dec in pH 10 to 167 mV/dec in 5 *M* HCl. Because the rate-determining step is unknown, especially on bare titanium, a variety of factors (rate-determining step, intermediate coverages, rate constants, etc.) may account for the observed Tafel slopes. Although it is known that the Tafel slope decreases with increasing pH, any mechanism that would account for this would be entirely speculative at this time.

The cathodic reaction is likely attributable to water reduction for the neutral and alkaline experiments, because hydrogen ion and oxygen reduction are unable to support such high current densities, even in the microsecond regime. Hydrogen ion reduction is likely charge-transfer controlled in this time frame in 5 *M* HCl. The cathodic Tafel slopes increase with increasing pH. The differences in Tafel slope could be accounted for by a change in the symmetry factor, β, or an entirely different reaction pathway when transitioning from hydrogen ion to water reduction with pH. A slow discharge-fast recombination mechanism has been proposed for film-covered titanium in acidic chloride solutions.[47] However, the reaction mechanism on bare titanium is likely different due to the presence of a bare metal surface instead of a semiconducting oxide. If the difference in cathodic Tafel slope with pH is due to a changing distance along the reaction path, *i.e.*, β, the water reduction reaction mechanism on bare titanium could be attributed to a conventional mechanism, such as the coupled discharge-recombination mechanism[48]

$$H^+ + e^- + M \xrightarrow{k_1} M - H_{ads} \quad [4]$$

$$M - H_{ads} + M - H_{ads} \xrightarrow{k_2} 2M + H_2 \quad [5]$$

Water reduction, in place of proton reduction (Eq. 4), is likely at neutral and alkaline pH. The current density for this reaction in 5 *M* HCl can be written as

$$i = k_1 C_{H^+}(1-\theta)\exp\left[\frac{-\beta\eta F}{RT}\right] = k_2\theta^2 \quad [6]$$

where θ is the surface coverage of H_{ads}, k_1 is a constant, and C_{H^+} is the H^+ concentration in solution. Assuming β = ½, a Tafel slope ranging from 120 (Langmuir) to 180 mV/dec (activated Temkin isotherm) is obtained for this mechanism. Of all the conventional hydrogen evolution reaction mechanisms, 180 mV/dec is the closest to those seen in Table IV. Larger Tafel slopes would be obtained for β < ½. Also, possible repulsive interactions between surface-adsorbed hydrogen atoms, at very high coverage on bare Ti, could also increase apparent Tafel slopes.

Variation of chloride concentration.—Chloride ion concentration is often a critical factor in electrochemical behavior of passive metals. Experiments were performed in 5 *M* LiCl (pH 3) to examine the effect of high chloride concentration without the extreme acidity of 5 *M* HCl (pH −1.64). Chloride concentrations less than 0.6 *M* were not examined, because the higher resistivity solutions would result in ohmic limitation of the peak current densities. Titanium thin films were fractured at applied potentials of 0 and −0.6 V_{SCE} as well as at open circuit in 5 *M* LiCl (Fig. 10). The bare surface OCP of the titanium film in 5 *M* LiCl is approximately 200 mV more positive than that in 0.6 *M* NaCl, as expected from its lower pH. This OCP falls along the OCP *vs.* pH line of Fig. 1, within experimental error. The peak current densities are slightly lower than those in 0.6 *M* NaCl at the same anodic overpotential but are not at theoretical ohmic current limits using Eq. 2 and 3. These results imply that either Cl^- or Li^+ weakly affects Ti/Ti^{+3} oxidation. Individual current transients were similar to those in 0.6 *M* NaCl, with roughly logarithmic decay. Therefore, for a given overpotential, repassivation behavior in 5 *M* LiCl appears to be similar to that in 0.6 *M* NaCl and is weakly dependent on chloride concentration for concentrations greater than 0.6 *M*.

Table IV. Comparison of parameters obtained by nonlinear least squares fitting of the bare surface polarization curves of Fig. 9. Reversible potentials were fixed during fitting. Exchange current densities (not reported) and Tafel slopes were allowed to vary. Anodic Tafel slope 2 is observed at low overpotential while anodic Tafel slope 1 is observed at high overpotential.

Solution	Anodic Tafel slope 1 (mV/dec)	Anodic Tafel slope 2 (mV/dec)	Cathodic Tafel slope (mV/dec)	Corrosion current density (A/cm^2)	OCP (V_{SCE})
5 *M* HCl	1600	167	182	8.1	−1.17
0.6 *M* NaCl	750	90.6	197	0.70	−1.58
0.6 *M* NaCl, pH 10	910	62.1	221	0.16	−1.60
d/*d*(pH)	—	−9.1	3.2	−0.15[a]	−0.039

[a] *d* [log(corrosion current density)]/*d* (pH).

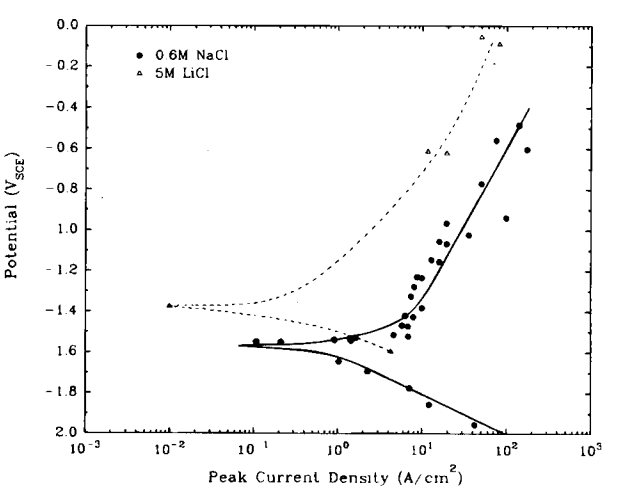

Fig. 10. Comparison of fractured titanium thin film peak current densities in 0.6 *M* NaCl and 5 *M* LiCl (pH 3).

Addition of $TiCl_3$.—Separate observations suggest that $TiCl_3$ is likely present in a crack tip solution. First, as discussed previously, the majority of charge passed following depassivation goes toward dissolution. Also, the presence of trivalent (rather than tetravalent) ions in solution has been noted following depassivation.[27] Moreover, an acidified crack tip solution (pH 1.7) has been observed following crack advance of an α-titanium alloy.[49] Hydrolysis of Ti^{3+} following film rupture, Cl^- migration toward the crack tip, and an accompanying decrease in solution pH with $TiCl_3$ concentration is expected. Appendix A discusses the expected hydrolysis for Ti^{3+}.

Thin film fracture tests were performed in 5 *M* HCl + 1 *M* $TiCl_3$ to examine the effect of $TiCl_3$ additions. Figure 11 compares peak current densities at applied potentials of 0 and −0.6 V_{SCE} in the $TiCl_3$ solution to 5 *M* HCl only. It appears that the bare surface peak current densities are lower in the solution with the added $TiCl_3$. The peak current density of the 0.6 V_{SCE} test in the $TiCl_3$ solution appears to be significantly lower than that in 5 *M* HCl alone. Figure 12 displays this more clearly, wherein tests in 5 *M* HCl show a higher peak current density at both smaller and larger anodic overpotentials. The peak current density at 0 V_{SCE} in 5 *M* HCl + 1 *M* $TiCl_3$ is only slightly lower than that in the 5 *M* HCl, however. Further, the OCP has been found to be about 160 mV more positive in the solution with additional $TiCl_3$.

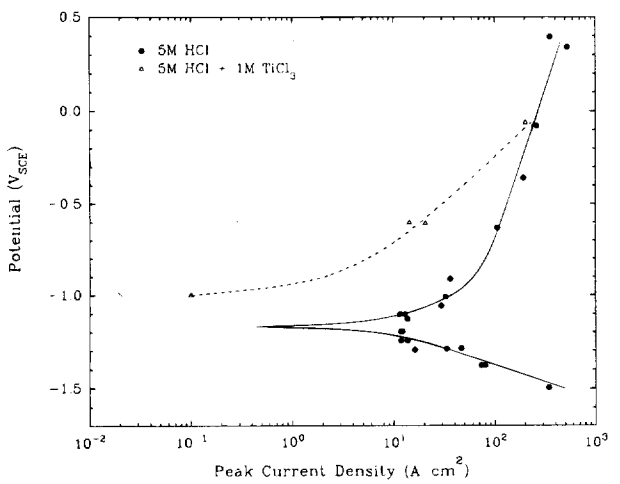

Fig. 11. Comparison of peak current densities of fractured titanium thin films exposed to 5 *M* HCl and 5 *M* HCl + 1 *M* $TiCl_3$.

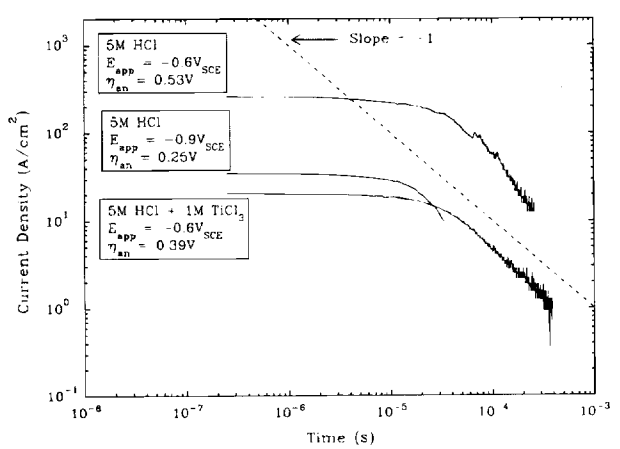

Fig. 12. Comparison of an individual current density transient in 5 *M* HCl + 1 *M* $TiCl_3$ to those in 5 *M* HCl only. The ohmically corrected overpotentials in 5 *M* HCl bracket the overpotential in the $TiCl_3$ solution. Overpotentials are with respect to the zero applied current condition at open circuit.

The effect of $TiCl_3$ on the repassivation behavior of fractured titanium alloy specimens has been previously examined.[14] Potentiostatic (E_{app} = 0.24 V_{NHE}) current transients in 3 *M* HCl and 3 *M* HCl saturated with $TiCl_3$ were compared. Although the data were ohmically limited, it was observed that the peak current density in the $TiCl_3$ solution was 25% of that in the HCl solution alone, even though the solution conductivity was 70% of that of the HCl solution. Moreover, it was stated that the rate of current decay appeared lower, suggesting a slower repassivation. This result is somewhat clouded by the ohmic limitation, which can affect the observed potentiostatic repassivation decay kinetics.[15,16] The OCP (obtained from the intersection of anodic and cathodic slopes) was found to be 300 to 400 mV more positive in the $TiCl_3$ solution compared to HCl.[14] It was concluded from these results that the presence of saturated $TiCl_3$ suppressed the anodic reaction.[14] The smaller positive shift in OCP seen here is likely due to differences in the concentration of $TiCl_3$ used.

Beck qualitatively described a change in repassivation behavior with the addition of $TiCl_3$.[14] This was confirmed by the present work. The slope of the current decay on the log *i* - log *t* plot was affected by the 1 *M* $TiCl_3$ addition. In the present work, *m* (Eq. 1) was found to be 1.3 to 1.4 (Table III) in 5M HCl. For the test in 5 *M* HCl + 1 *M* $TiCl_3$ in Fig. 12, however, *m* was 1.14. Thus, the anodic current density decays more slowly in the $TiCl_3$ solution, as proposed by Beck.[14] Therefore, the present results confirm the results of earlier work,[14] namely, that significant additions of $TiCl_3$ reduce the peak current density on bare titanium surfaces, inhibit anodic reactions, and slow repassivation. These findings appear consistent with those of Wanhill who found that $TiCl_3$ slowed stage II stress corrosion crack growth rates.[52]

Comparison of Scratch Depassivation and Fractured Thin Film Data

Bare surface polarization curves for the six alloys were each generated in 5 *M* HCl, 0.6 *M* NaCl, and 0.6 *M* NaCl adjusted to pH 10 by scratch repassivation. Figure 13 compares the six different materials in 0.6 *M* NaCl, the lines being a qualitative best fit through the data. As before, potentials are ohmically corrected utilizing the solution resistance calculated from Eq. 3 (approximately 280 Ω). Within the limitations of the scratch test, little difference is observed between the anodic bare surface repassivation

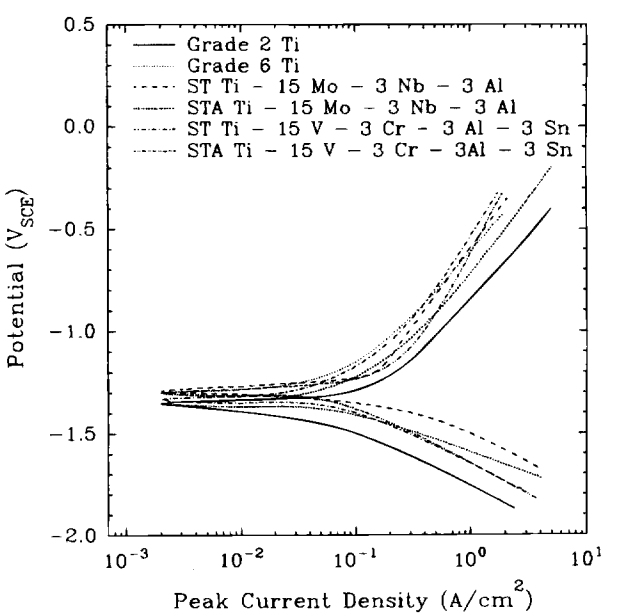

Fig. 13. Comparison of the bare surface (peak current) polarization behaviors after scratching of six different α, β, and β + α alloys exposed to 0.6 *M* NaCl.

behavior of all of the alloys examined, regardless of chemical composition or microstructure. Peak currents, OCP, total anodic charges, and repassivation rates were all comparable as well, except for grade 2 Ti which consistently yielded a higher charge density per repassivation event at every potential (Table V). Results were analogous in the acidic and alkaline solutions also. A single test performed with STA Ti-3Al-8V-6Cr-4Zr-4Mo (0.6 *M* NaCl, E_{app} = 0.6 V_{SCE}) yielded a similar peak current density and slightly lower anodic charge density than those seen for STA Ti-15Mo-3Nb-3Al and STA Ti -15V-3Cr-3Al-3Sn.

A bare surface polarization curve resulting from scratch testing (grade 2 titanium) is compared to fractured thin film data (evaporated from pure Ti target) in Fig. 14. Scratch depassivation testing appears to qualitatively show the same results as for fractured thin films. Quantitatively, however, there are differences between fractured thin film and scratch tests. The scratch test peak current densities are one to two orders of magnitude lower than those arising from fractured thin films, as predicted.[15] The OCP is 250 mV more noble as well, because significant repassivation has occurred at the start of the scratch by the time the end of the scratch is reached.

The qualitative similarity between thin film and scratch tests was further investigated by comparing scratch test polarization curves on grade 2 titanium (peak current density) from solutions of varying pH (Fig. 15). As with thin film experiments (Fig. 9), the bare surface anodic polarization curves display two distinct regions of shallow and steep slope. The cathodic Tafel slope is also steep, relative to that seen at steady state.[6,7] The OCPs are all approximately 250 mV more positive than those obtained from the fractured films. The differences in OCP between solutions are similar, in general, regardless of depassivation method. The OCP was found to decrease approximately 50 mV/pH (in tests from pH −1.64 to 14, not shown), a magnitude slightly larger than that seen with thin films (Fig. 1). Moreover, the corrosion current density appears to be about an order of magnitude higher in 5 *M* HCl than in the neutral and pH 10 solutions, as seen previously (Fig. 9 and Table IV). Therefore, it appears that scratch tests adequately predict repassivation trends on titanium, albeit in a strictly qualitative manner. With this result, comparison between repassivation behaviors of various alloys using the scratch method can be undertaken with an increased level of confidence .

Figure 16 is a plot of bare surface polarization curves on STA Ti-15Mo-3Nb-3Al exposed to 0.6 *M* NaCl at various times following depassivation. As with fractured thin films, the observed bare surface current density is much

Table V. Comparison of scratch test charge densities on various alloys exposed to different solutions. Charge densities were calculated by integrating the first 90 ms of the current transient from the peak current density.

Solution	Applied potential	Material	Charge density (mC/cm²)
0.6 *M* NaCl	−0.6 V_{SCE}	STA Ti-15Mo-3Nb-3Al	3.4
	−0.6 V_{SCE}	Grade 2	5.0
	−0.6 V_{SCE}	ST 15V-3Cr-3Al-3Sn	3.6
	−0.6 V_{SCE}	ST Ti-15Mo-3Nb-3Al	3.4
	−0.6 V_{SCE}	STA Ti-15V-3Cr-3Al-3Sn	3.3
	−0.6 V_{SCE}	Grade 6	2.7
	−0.6 V_{SCE}	STA Ti-3Al-8V-6Cr-4Zr-4Mo	2.3
	−1 V_{SCE}	STA Ti-15Mo-3Nb-3Al	0.76
	−0.9 V_{SCE}[a]	Grade 2	1.8
5 *M* HCl	−0.6 V_{SCE}	STA Ti-15Mo-3Nb-3Al	4.7
	−0.6 V_{SCE}	Grade 2	6.0
0.6 *M* NaCl pH 10	−0.6 V_{SCE}	STA Ti-15Mo-3Nb-3Al	5.7
	−0.6 V_{SCE}	Grade 2	6.9
	−1 V_{SCE}	STA Ti-15Mo-3Nb-3Al	0.49
	−1 V_{SCE}	Grade 2	1.4

[a]No experiment performed at −1 V_{SCE}. Charge density atom from E_{app} = −0.9 V_{SCE} is shown instead.

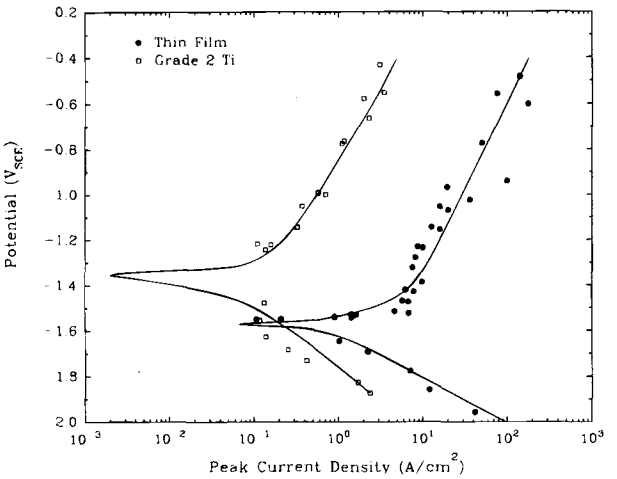

Fig. 14. Comparison of bare surface (peak current) polarization curves utilizing fractured titanium thin films and scratch testing on grade 2 titanium in 0.6 *M* NaCl.

larger than that seen during "steady-state" potentiodynamic tests. The OCP and current density shift over time toward those seen at steady state, similar to that observed with fractured thin films (Fig. 5). The 5 ms E − log i plots for grade 2 and STA Ti-15V-3Cr-3Al-3Sn are also shown in Fig. 16. The behavior of these alloys at 5 ms, as well as all of the other alloys examined at 5 ms, was similar. The repassivation E − log i behaviors of all of the alloys at 5 ms and other longer times (not shown) are all still similar at times beyond which depassivation speed or other experimental factors limit peak current densities.[15]

Others have also noted similar anodic repassivation behavior between commercially pure titanium, Ti-8-1-1, and Ti-14 Mo.[14] Two factors likely account for the similar repassivation behaviors of the different titanium alloys in aqueous chloride solutions. The predominance of TiO_2 in all of the oxide films and Ti/Ti^{+3} dissolution following repassivation[6,7] likely contributes to the similar results. At the more negative potentials examined here, oxides of the major alloying elements found in Ti-15Mo-3Nb-3Al and Ti-15V-3Cr-3Al-3Sn; Mo and V, respectively,[6,7,24] are not thermodynamically stable (assuming metal ion concentrations of 10^{-6} *M* and pH 6). The reversible potentials for stable oxidation states of Mo and V are shown in Fig. 16. Therefore, these oxides cannot contribute to repassivation.

The charge (Table V) and peak current (Fig. 13) densities for grade 6 Ti, which approximates the composition of the α precipitates within the β matrix, were similar to those of

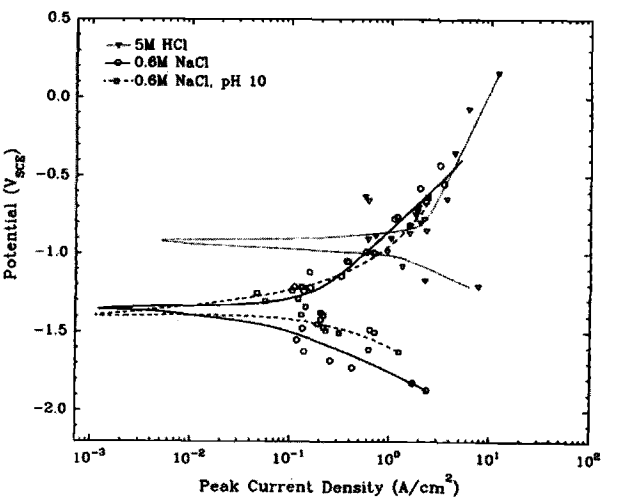

Fig. 15. Bare surface polarization curves on grade 2 titanium in different solutions obtained by scratch testing.

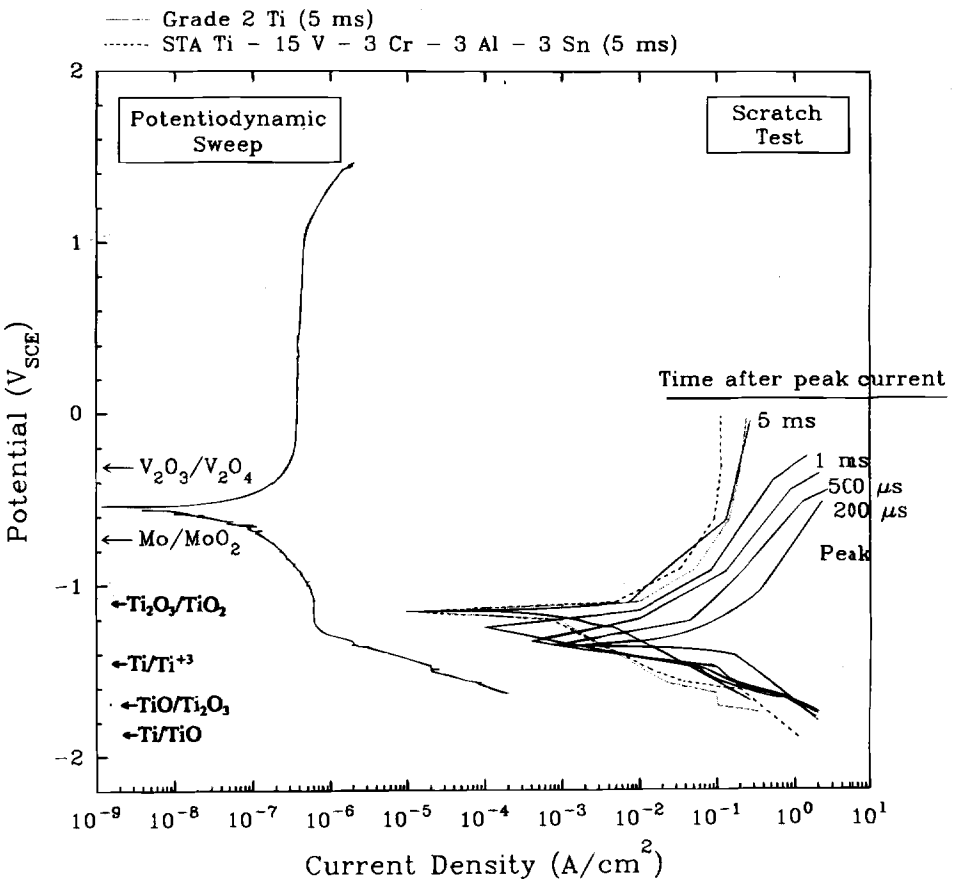

Fig. 16. Polarization curves of STA Ti-15Mo-3Nb-3Al in 0.6 *M* NaCl at various times following scratch depassivation. STA Ti-15V-3Cr-3Al-3Sn and grade 2 polarization curves in 0.6 *M* NaCl at 5 ms after depassivation are also shown. Reversible potentials for the oxidation of major alloying components are also shown at a pH of 6 and 10^{-6} *M* metal ion concentrations.

the ST β alloys. This indicates that α precipitates in a β + α alloy containing similar Al and V contents as grade 6 Ti may behave similarly to the β matrix when the passive film is destabilized at room temperature. In summary, it appears that less than 15 w/o differences in composition and microstructure have little effect on the repassivation behavior of a β-titanium alloy. Observed differences in EAC susceptibility between alloys do not appear to result from differences in repassivation behavior of β- *vs.* α-Ti. However, high segregated Al concentrations may exert a negative influence on the passivity and repassivation of Ti.[54]

Conclusions

The repassivation behavior of titanium in aqueous chloride environments has been examined to obtain a better understanding of observed EAC behavior under dynamic strain. The bare surface OCP was found to decrease 43 mV/pH unit. Current densities greater than 100 A/cm^2 were observed upon fracture of titanium thin films in 0.6 *M* NaCl. The large majority of anodic charge during repassivation contributed to dissolution of titanium and not film formation. It was shown that significant dissolution takes place over the length of the current decay transient. Little difference was seen in the repassivation behavior of titanium in acidic, alkaline, and neutral chloride solutions. Similar behaviors in solutions of widely varying pH argues against a slip-film rupture-dissolution mechanism controlling EAC of β-titanium alloys, as crack initiation is observed when acidic crack tip chemistries are present, but not when alkaline chemistries exist. 5 *M* LiCl lowered peak current densities but did not affect repassivation behavior. Repassivation experiments performed in 5 *M* HCl + 1 *M* $TiCl_3$ found that $TiCl_3$ lowered peak current densities and slowed repassivation. Scratch depassivation tests indicate that little difference exists between the repassivation behaviors of selected β-titanium alloys. Tests comparing EAC-immune and susceptible alloys, *e.g.*, ST *vs.* STA Ti-15Mo-3Nb-3Al or STA Ti-15Mo-3Nb-3Al *vs.* STA Ti-15V-3Cr-3Al-3Sn, showed similar behavior, indicating that EAC susceptibility is not controlled by readily apparent alloy-specific differences in repassivation behavior. Grade 6 Ti yielded identical behavior to the ST β-titanium alloys, indicating little difference in repassivation behavior between the β-matrix and the α-precipitates in the STA alloys containing small concentrations of Al and V.

Acknowledgment

The authors acknowledge the Office of Naval Research (Grant No. N00014-91-J-4164) and the Virginia Center for Innovative Technology for their support of this work. The authors also thank TIMET and RMI for their generous donation of alloys. Further, we would like to acknowledge R.G. Kelly, E. Gileadi, and L. L. Scribner for their helpful discussions.

Manuscript submitted June 9, 1995; revised manuscript received March 12, 1996.

APPENDIX A

Crack tip solution acidification following cracking has been observed.[49] Solution acidification can be explained as follows. Trivalent titanium is produced following depassivation.[27] The trivalent titanium may then hydrolyze. Two hydrolysis reactions of Ti^{3+} are possible[50]

$$(i)\ Ti^{3+} + H_2O \rightleftharpoons TiOH^{2+} + H^+$$

$$(ii)\ 2Ti^{3+} + 2H_2O \rightleftharpoons Ti_2(OH)_2^{4+} + 2H^+ \qquad [A\text{-}1]$$

Using published hydrolysis constants,[50] a distribution diagram of hydrolysis products can be calculated for Ti^{3+} ions, similar to that for other ions.[50,51] Figure A-1 shows the distribution diagram (assuming the activity coefficient of $H^+ = 1$ at all pH, which is not a good assumption at low pH) for trivalent titanium at ionic strength, *I*, of 1 mol/kg H_2O. The distribution diagram for $I = 3$ mol/kg H_2O (not shown) is nearly identical, with the curves shifted slightly to the left. The ionic strength, *I*, is defined as[50]

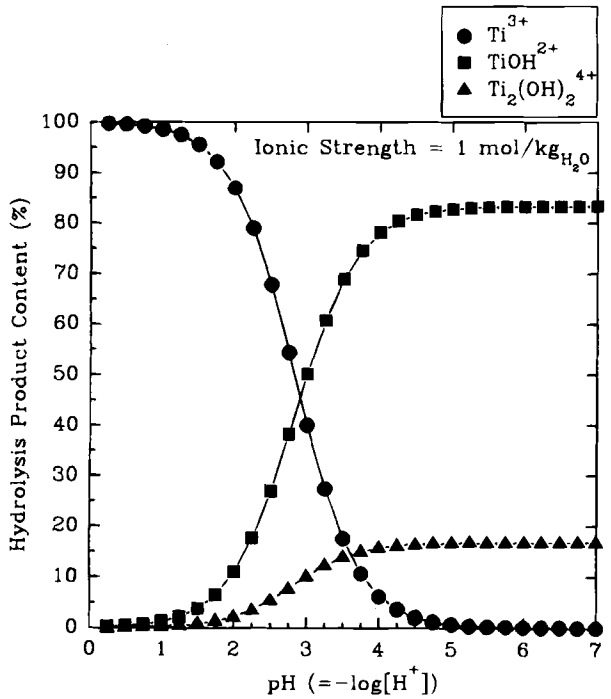

Fig. A-1. Distribution diagram for Ti^{3+} and its hydrolysis products.

$$I = \frac{\sum z_i^2[i]}{2} \qquad [A\text{-}2]$$

where z and i are the charge and concentration, respectively, of each individual species. Figure A-1 assumes titanium ion additions to 0.6 *M* NaCl, such that 0.6 of the 1 mol/kg H_2O ionic strength is attributable to sodium and chloride ions added as NaCl. The distribution diagram indicates that Ti^{3+} additions to neutral 0.6 *M* NaCl solution readily hydrolyze and that $TiOH^{2+}$ is the dominant hydrolysis product. To confirm this calculation, $TiCl_3$ was added to distilled, deionized water in an inert atmosphere and the pH recorded. Concentrations of 10^{-4} to 1 *M* $TiCl_3$ were examined (see Fig. A-2). The pH of the solution was found to decrease from neutral to about pH 3 when 10^{4} *M* $TiCl_3$ was added. At 1 *M* $TiCl_3$, the pH approached 0.

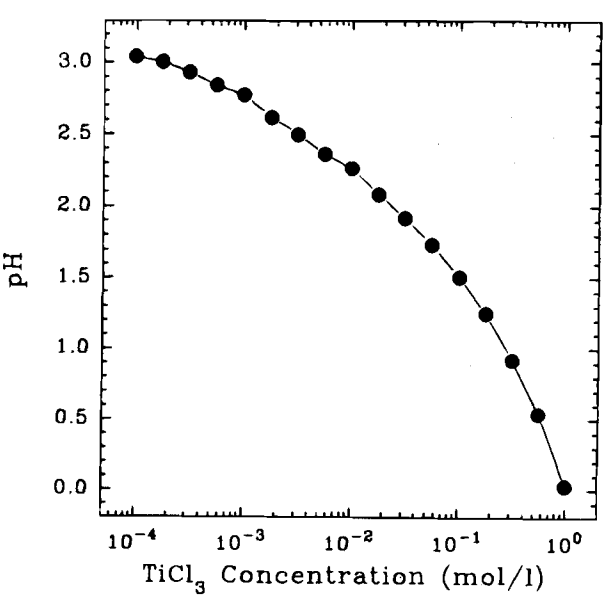

Fig. A-2. Variation of measured pH for various $TiCl_3$ concentrations in distilled, deionized water in an inert atmosphere.

REFERENCES

1. L. M. Young, G. A. Young, Jr., J. R. Scully, and R. P. Gangloff, *Metall. Trans. A*, **26A**, 1257 (1995).
2. L. M. Young, M. S. Thesis, University of Virginia, Charlottesville, VA (1993).
3. B. P. Somerday, J. P. Grandle, and R. P. Gangloff, in *Proceedings of the Tri-Service Conference on Corrosion*, p. 375, Materials Laboratory, Wright Patterson Air Force Base, OH (1994).
4. G. A. Young, *Scr. Metall.*, **28**, 507 (1993).
5. F. P. Ford, *Met. Sci.*, 326 (1978).
6. D. G. Kolman and J. R. Scully, *This Journal*, **140**, 2771 (1993).
7. D. G. Kolman and J. R. Scully, *ibid.*, **141**, 2633 (1994).
8. T. R. Beck, *ibid.*, **115**, 890 (1968).
9. T. R. Beck, in *Passivity of Metals*, R. P. Frankenthal and J. Kruger, Editors, p. 1035, The Electrochemical Society Corrosion Monograph Series, Princeton, NJ (1978).
10. H. J. Rätzer-Scheibe, in *Passivity of Metals and Semiconductors*, M. Froment, Editor, p. 731, Elsevier Science Publishers, Amsterdam (1983).
11. H. J. Rätzer-Scheibe, in *Proceedings of the 8th International Congress on Corrosion*, p. 212, Mainz, Germany (1981).
12. H. J. Rätzer-Scheibe and H. Buhl, in *Titanium Science and Technology - Proceedings of the 5th International Conference on Titanium*, G. Lütjering, U. Zwicker, and W. Bunk Editors, Vol. 4, p. 2641, Deutsche Gesselschaft für Mettalkunde, Germany (1984).
13. I. A. Ammar and I. Kamal, *Electrochim. Acta*, **16**, 1539 (1971).
14. T. R. Beck, *ibid.*, **18**, 815 (1973).
15. D. G. Kolman and J. R. Scully, *This Journal*, **142**, 2179 (1995).
16. G. T. Burstein and A. J. Davenport, *ibid.*, **136**, 936 (1989).
17. G. S. Frankel, B. M. Rush, V. A. Brusic, S. M. Mirzamaani, and A. J. Davenport, in *Corrosion of Electronic Materials and Devices*, J. D. Sinclair, Editor, PV 91-2, p. 263, The Electrochemical Society Proceedings Series, Pennington, NJ (1991).
18. G. S. Frankel, B. M. Rush, C. V. Jahnes, C. E. Farrell, A. J. Davenport, and H. S. Isaacs, *This Journal*, **138**, 643 (1991).
19. A. J. Davenport and H. S. Isaacs, in *Transient Techniques in Corrosion Science and Engineering*, W. H. Smyrl, D. D. Macdonald, and W. J. Lorenz, Editors, PV 89-1, p. 357, The Electrochemical Society Proceedings Series, Pennington, NJ (1989).
20. P. D. Bastek, R. C. Newman, and R. G. Kelly, *This Journal*, **140**, 1884 (1993).
21. H. J. Pearson, G. T. Burstein, and R. C. Newman, *ibid.*, **128**, 2297 (1981).
22. P. O. Gartland, SINTEF Publication STF16-A88085, Trondheim, Norway (1988).
23. T. R. Beck, in *Proceeding of the Conference on Fundamental Aspects of Stress Corrosion Cracking*, R. W. Staehle, A. J. Forty, and D. VanRooyen, Editors, p. 608, NACE, Houston, TX (1969).
24. (a) D. C. Silverman, *Corrosion*, **38**, 541 (1982); (b) J. W. Olver and J. W. Ross, Jr., *J. Am. Chem. Soc.*, **85**, 2565 (1963); (c) G. B. Naumov, B. N. Ryzhenko, and I. L. Khodakawsky, *Handbook of Thermodynamic Data*, USGS Translation, USGS-WRD-74-000 (1974); (d) D. D. Wagman, NBS Technical Note 270-3, 270-5 (1971); (e) D. P. Feldman, V. M. Berdonikov, and B. P. Matseevskii, *Russ. J. Phys. Chem.*, **49**, 1858 (1975).
25. *Atlas of Electrochemical Equilibria in Aqueous Solutions*, M. Pourbaix, 2nd ed., NACE, Houston, TX (1974).
26. M. Pourbaix, in *The Theory of Stress Corrosion Cracking*, J. C. Scully, Editor, p. 17, NATO Scientific Affairs Division, Brussels, Belgium (1971).
27. T. R. Beck, *Electrochim. Acta*, **18**, 807 (1973).
28. M. Fleischmann and H. R. Thirsk, in *Advances in Electrochemistry and Electrochemical Engineering*, Vol. 3, P. Delahay and C. W. Tobias, Editors, p. 123, John Wiley & Sons, Inc., New York (1963).
29. D. Laser, M. Yaniv, and S. Gottesfeld, *This Journal*, **125**, 358 (1978).
30. J. R. Ambrose and J. Kruger, *ibid.*, **121**, 599 (1974).

31. F. P. Ford, *J. Pressure Vessel Technol.*, **110**, 113 (1988).
32. N. F. Cabrera and N. F. Mott, *Rep. Prog. Phys.*, **12**, 163 (1948/1949).
33. B. MacDougall, *This Journal*, **130**, 114 (1983).
34. T. R. Beck, *Corrosion*, **30**, 408 (1974).
35. T. R. Beck and E. A. Grens II, *This Journal*, **116**, 177 (1969).
36. G. T. Burstein and D. H. Davies, *ibid.*, **128**, 33 (1981).
37. G. T. Burstein and P. I. Marshall, *Corros. Sci.*, **23**, 125 (1983).
38. L. I. Krishtalik, in *Comprehensive Treatise of Electrochemistry, Kinetics and Mechanisms of Electrode Processes*, B. E. Conway, J. O'M. Bockris, E. Yeager, S. U. M. Khan, and R. E. White, Editors, Vol. 7, p. 87, Plenum Press, New York (1983).
39. R. Audubert, *Discuss. Faraday Soc.*, **1**, 72 (1947).
40. D. G. Kolman, Ph.D. Thesis, University of Virginia, Charlottesville, VA (1996).
41. M. J. Blackburn, J. A. Feeney, and T. R. Beck in *Advances in Corrosion Science and Technology*, M. G. Fontana, Editor, Vol. 3, p. 67, Plenum Press, New York (1972).
42. A. Caprani, J. P. Frayret, R. Pointeau, S. K. Marya, and F. Le Maitre, *Electrochim. Acta*, **28**, 141 (1983).
43. A. Caprani and J. P. Frayret, J. Less-Common Met., **69**, 29 (1980).
44. A. Caprani and J. P. Frayret, *Electrochim. Acta*, **24**, 835 (1979).
45. J. P. Frayret and A. Caprani, *ibid.*, **27**, 391 (1982).
46. J. P. Frayret, A. Caprani, T. Jaszay, and F. Priem, *Corrosion*, **41**, 656 (1985).
47. E. J. Kelly and H. R. Bronstein, *This Journal*, **131**, 2232 (1984).
48. P. K. Subramanyan, in *Comprehensive Treatise of Electrochemistry*, J. O'M. Bockris, Editor, Vol. 4, p. 411, Plenum Press, New York (1981).
49. B. F. Brown, C. T. Fujii, and E. P. Dahlberg, *This Journal*, **116**, 218 (1969).
50. C. F. Baes, Jr. and R. E. Mesmer, *The Hydrolysis of Cations*, Krieger Publishing Co., Malabar, FL (1986).
51. R. G. Buchheit, J. P. Moran, and G. E. Stoner, *Corrosion/90*, Paper No. 93, NACE, Houston, TX (1990).
52. R. J. H. Wanhill, *Br. Corros. J.*, **10**, 69 (1975).
53. B. D. Lichter, R. M. Bhatkal, and W. F. Flanagan, in *Parkins Symposium on Fundamental Aspects of SCC*, S. Bruemmer, Editor, p. 270, TMS, Warrendale, PA (1992).
54. T. Yu and J. R. Scully, Submitted to *Corrosion* (March 1996).

Oxidation Kinetics of Water and Organic Compounds by Silver (II) Using a Potentiometric Method

Albert Lehmani, Pierre Turq, and Jean-Pierre Simonin

Laboratoire d'Electrochimie URA 430, Université Pierre et Marie Curie, 75252 Paris Cedex 05, France

ABSTRACT

A new experimental method using an electrochemical technique is presented for the study of the oxidation kinetics of water and organic compounds. The electrogeneration of silver (II) in 6 *M* nitric acid is presented. Good agreement is found between a theoretical model and the experimental results. Since the Ag(II)/Ag(I) system obeys Nernst's law, the potential of this couple can be followed as a function of time. This technique has been used to study the oxidation kinetics of water, formic acid, acetic acid, and urea by silver (II) in 6 *M* nitric acid. The reactions were found to be first order with respect to organic compounds. Oxidation kinetics of formic acid and acetic acid showed first order in silver (II) and that of urea was found to be second order in silver (II).

Introduction

Silver (II) is known for being one of the most powerful oxidizing agents in acidic media. It is more oxidizing than the Co(III), Mn(II), or Ce(IV) ions and can be used for the destruction of organic compounds or the dissolution of nuclear wastes.[4,7,13-15] The potential of the Ag(II)/Ag(I) couple *vs.* the normal hydrogen electrode (NHE) lies between 1.91 V/NHE and 1.96 V/NHE in nitric acidic media.[1,2] Besides, this potential is superior to the thermodynamic potential of water (1.23 V/NHE). The silver (II) ion is then unstable in aqueous media and oxidizes water according to a complex mechanism described by Po *et al.*[3] Some authors[4,5] have studied the kinetics of the oxidation of silver (I) into silver (II) in nitric acid media. They showed that the Ag(II)/Ag(I) system is fast and reversible using various electrochemical techniques.

Many authors have described the kinetics and mechanisms of oxidation of metals and various organic compounds by silver (II) using spectroscopic techniques.[6-12] In the present paper, a new technique is presented, which is based on a potentiometric method. Our study relies on the observation that since Nernst's law is applicable to the Ag(II)/Ag(I) system, the potential of this couple can be followed as a function of time (potentiometric method). Using a simple and accurate electrochemical technique, it is thus possible to determine the oxidation kinetics of the solvent and of various organic compounds by silver (II). We can also determine the kinetics of silver (II) electrogeneration by a simple potentiometric measurement. This study first focuses on the kinetics of water oxidation and then on the oxidation kinetics of organic compounds such as formic acid, acetic acid, and urea.

Kinetic Models

Generation of silver (II).—The electrolysis of a silver (I) solution in nitric acid is known to consist of the following reaction steps[4,13,14,15]

In the anodic compartment, the silver (II) ion that is produced oxidizes water

$$Ag^+ \rightarrow Ag^{2+} + e^-$$

$$2H_2O \rightarrow O_2 + 4H^+ + 4e^-$$

$$2Ag^{2+} + H_2O \rightarrow 2Ag^+ + 2H^+ + 1/2\ O_2$$

In the cathodic compartment, the global reaction is

$$HNO_3 + 2H^+ + 2e^- \rightarrow HNO_2 + 2H_2O$$

The nitrous acid HNO_2 produced at the cathode migrates through the separator and reduces silver (II) in the anodic compartment

$$2Ag^{2+} + HNO_2 + H_2O \rightarrow HNO_3 + 2Ag^+ + 2H^+$$

This reaction leads to a decrease in the chemical efficiency for the production of silver (II). Thus it is necessary to put a separator between the two compartments that is able to "stop" the undesired species.